PAPER • **OPEN ACCESS**

Local random vector model for semiclassical fractal structure of chaotic resonance states

To cite this article: Konstantin Clauß and Roland Ketzmerick 2022 *J. Phys. A: Math. Theor.* **55** 204006

OPEN ACCESS
IOP Publishing
Journal of Physics A: Mathematical and Theoretical
J. Phys. A: Math. Theor. **55** (2022) 204006 (24pp)
https://doi.org/10.1088/1751-8121/ac62b9

Local random vector model for semiclassical fractal structure of chaotic resonance states

Konstantin Clauß[1,2] **and Roland Ketzmerick**[1,*]

[1] Institut für Theoretische Physik and Center for Dynamics, Technische Universität Dresden, 01062 Dresden, Germany
[2] Department of Mathematics, Technical University of Munich, Boltzmannstraße 3, 85748 Garching bei München, Germany

E-mail: roland.ketzmerick@tu-dresden.de

Received 24 December 2021, revised 3 March 2022
Accepted for publication 30 March 2022
Published 21 April 2022

Abstract

The semiclassical structure of resonance states of classically chaotic scattering systems with partial escape is investigated. We introduce a local randomization on phase space for the baker map with escape, which separates the smallest multifractal scale from the scale of the Planck cell. This allows for deriving a semiclassical description of resonance states based on a local random vector model and conditional invariance. We numerically demonstrate that the resulting classical measures perfectly describe resonance states of all decay rates γ for the randomized baker map. By decreasing the scale of randomization these results are compared to the deterministic baker map with partial escape. This gives the best available description of its resonance states. Quantitative differences indicate that a semiclassical description for deterministic chaotic systems must take into account that the multifractal structures persist down to the Planck scale.

Keywords: quantum chaos, semiclassical limit, resonance states, random vector model, local randomization

(Some figures may appear in colour only in the online journal)

*Author to whom any correspondence should be addressed.

1. Introduction

Understanding the correspondence of quantum and classical dynamics is an essential task in complex systems [1]. Most prominently, the semiclassical structure of quantum eigenstates in closed systems is related to classically invariant phase-space structures [2–4]. For classically ergodic dynamics almost all quantum eigenstates converge weakly towards the uniform measure on phase space as proven by the quantum ergodicity theorem [5–9]. This uniform limit is also established for quantum maps [10–12]. The amplitude distribution of eigenstates is described by random wave models, first introduced for quantum billiards [2], in which a complex Gaussian distribution of wave amplitudes leads to a universal exponential distribution of the intensities [12–19]. Extensions include constraints by two-point correlations [20–22] and systems with a mixed phase space [23, 24].

In contrast, for systems with loss of particles or intensity in some interaction region [25] the semiclassical limit is not fully understood. Such scattering systems, e.g., the three-disk system [26–28] or optical microcavities [29], are described by resonance poles and the corresponding resonance states ψ which have a decay rate γ. The distribution of decay rates is well described by a fractal Weyl law in systems with full escape [30–38], and has been studied in systems with partial escape [39–42]. Here we focus on the semiclassical structure of resonance states in chaotic systems with escape. They are described by multifractal measures on phase space [43–55] with exponentially distributed intensity fluctuations [56]. These measures are conditionally invariant under the classical dynamics with escape [25, 57] and strongly depend on the corresponding quantum decay rate γ [46, 53, 54]. Such questions are also of interest in mixed systems and in non-Hermitian PT-symmetric systems [58–61]. For fully chaotic systems there exist approximative descriptions of resonance states with arbitrary decay rates γ for full [53] and partial escape [54], however, the precise semiclassical limit is not known.

The main difficulty in describing chaotic resonance states, according to our understanding, is the fact that their multifractal structures persist all the way down to the scale of a Planck cell. Since the multifractal structure has its origin in the classical dynamics, there is no separation of the smallest classical scale and the scale of a Planck cell, not even when going to the semiclassical limit.

In this paper we introduce a chaotic model system with escape for which the smallest multifractal scale and the scale of the Planck cell are separated. This allows for deriving a semiclassical description of resonance states. Specifically, we define the randomized baker map with escape, where in addition to the quantum baker map and escape from phase space, local randomization operations on phase space with an adjustable scale are applied. Resonance states show multifractal structures on scales larger than the scale of randomization and are uniformly fluctuating on smaller scales. For partial escape, we derive classical measures, which (i) are conditionally invariant with some desired decay rate γ on scales larger than the scale of randomization and (ii) obey an extremum principle derived from a local random vector model in each randomization region. We numerically demonstrate that for all decay rates γ these classical measures perfectly describe resonance states in the semiclassical limit. By decreasing the scale of randomization these results are compared to the deterministic baker map with partial escape. This gives the best available description of its resonance states. Quantitative differences indicate that a semiclassical description for deterministic chaotic systems must take into account that the multifractal structures persist down to the Planck scale.

The paper is organized as follows. In section 2 we review the classical baker map and its symbolic dynamics. Section 3 introduces the randomized quantum baker map with escape and discusses the structure of its resonance states. In section 4 we determine classical measures from a local random vector model with the constraint of conditional invariance. We conjecture

that these classical measures describe the semiclassical structure of resonance states. Numerical support for the conjecture is presented in section 5. A comparison to the deterministic quantum baker map is made in section 6 showing qualitative similarity, but quantitative difference. Section 7 gives an outlook and in appendix C a random matrix model with escape is discussed.

This paper touches many topics that Haake has worked on [1], as it studies the semiclassical limit of a quantum model combining classical deterministic chaotic dynamics with random matrices. Specifically, the local randomization procedure is related to the blurring of phase-space resolution studied by Haake [62–64]. Furthermore the present paper deals with open quantum systems, another field to which Haake contributed substantially in terms of scattering systems [65, 66], as well as in terms of coupling to a thermal environment [67, 68]. It would have been a pleasure to discuss the results with Haake and to carefully listen to his insights.

2. Classical baker map with escape

In this section we introduce the baker map, one of the paradigmatic models for chaos, combined with escape from phase space [25, 69]. Its symbolic dynamics will be used to define a phase-space partition with rectangles that will be relevant for the randomized quantum baker map with escape introduced in the next section.

2.1. Baker map with escape

The baker map with n stripes is defined on the two-torus $\mathbb{T} = [0,1) \times [0,1)$ as follows [70]. Consider the vertical rectangles $A_k = [k/n, (k+1)/n) \times [0,1)$ for $k \in \{0, \ldots, n-1\}$. The n-baker map compresses each of these rectangles along the p-direction by the factor $1/n$ and stretches it along the horizontal q-direction by the factor n, after which they are stacked on top of each other,

$$\begin{aligned} &B_n : \mathbb{T} \to \mathbb{T} \\ &A_k \ni (q,p) \mapsto \big(qn - k, (p+k)/n\big)\,. \end{aligned} \tag{1}$$

Note that B_n is volume preserving on $\mathbb{T}$.

For the baker map with escape we consider a loss of intensity which is constant in each of the rectangles A_k. In particular, let $\boldsymbol{r} \in \mathbb{R}_+^n$ and define the reflectivity function $r : \mathbb{T} \to \mathbb{R}_+$ as $A_k \ni (q,p) \mapsto r_k$, see figure 1(a). Extending the phase space with the intensity space $\mathbb{R}_+$, the map with escape is defined by

$$\begin{aligned} &B_{n,\boldsymbol{r}} : \mathbb{T} \times \mathbb{R}_+ \to \mathbb{T} \times \mathbb{R}_+ \\ &((q,p), I) \mapsto (B_n(q,p), I \cdot r(q,p)), \end{aligned} \tag{2}$$

i.e., the intensity in A_k is changed by the factor r_k. One distinguishes systems with full escape, where at least one of the $r_k = 0$, from systems with partial escape, where all $r_k > 0$ [25]. Often $r_k \leqslant 1$ is considered, leading to classical decay under the forward map [25]. On the other hand, considering $r_k \geqslant 1$ for some (or all) A_k implies growth of intensities [71]. The simple structure of the baker map with escape allows for determining the natural decay rates under forward and backward dynamics analytically. The natural measure is uniform along the unstable q-direction such that the natural decay rate is given by $\gamma_{\text{nat}} = -\ln(\frac{1}{n}\sum_{k=0}^{n-1} r_k)$ [72]. The natural measure of the backward dynamics is uniform along the stable p-direction, such that the natural growth rate of the inverse map is $\gamma_{\text{inv}} = \ln(\frac{1}{n}\sum_{k=0}^{n-1} \frac{1}{r_k})$ [54, 71]. Another important classical

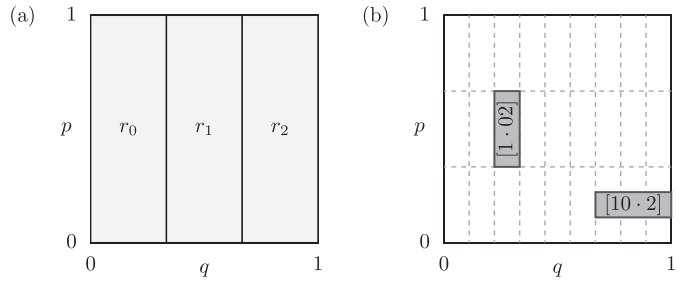

Figure 1. (a) Illustration of reflectivities r_k in rectangles A_k for the three-baker map with escape. (b) Phase-space partition by rectangles $[\boldsymbol{\alpha}_{m_p,m_q}]$ with $m_p = 1$ and $m_q = 2$ shown by dashed lines. The rectangle $[1 \cdot 02]$ and its iterate $[10 \cdot 2]$ are highlighted, where the latter intersects with three rectangles of the partition.

decay rate is the average decay of a typical ergodic orbit [40], the so-called typical decay rate $\gamma_{\text{typ}} = -\frac{1}{n}\sum_{k=0}^{n-1} \ln r_k$. One has the ordering $\gamma_{\text{nat}} \leqslant \gamma_{\text{typ}} \leqslant \gamma_{\text{inv}}$, with equality if all r_k are identical.

2.2. Symbolic dynamics and phase-space partition

The baker map has a complete symbolic dynamics in terms of the Markov partition $\{A_k\}_{k=0}^{n-1}$. Therefore it is equivalent to a shift on symbolic sequences, which is recalled in the following. Let S be the right shift operator on the symbolic space $Z_n = \{0, 1, \ldots, n-1\}^{\mathbb{Z}}$, which consists of bi-infinite sequences $\boldsymbol{\alpha} = \{\alpha_i\}_{i=-\infty}^{\infty} = \ldots \alpha_{-2}\alpha_{-1} \cdot \alpha_0\alpha_1\alpha_2 \ldots$, where $\alpha_i \in \{0, \ldots, n-1\}$ for all $i \in \mathbb{Z}$. The shift operator $S : Z_n \to Z_n$ acts on such sequences as

$$S(\boldsymbol{\alpha}) = \ldots \alpha_{-2}\alpha_{-1}\alpha_0 \cdot \alpha_1\alpha_2 \ldots, \tag{3}$$

i.e., it shifts the center of this sequence by one such that $(S(\boldsymbol{\alpha}))_i = \alpha_{i+1}$. There is a mapping from the space of symbolic sequences to the torus, $J_n : Z_n \to \mathbb{T}$,

$$J_n(\boldsymbol{\alpha}) = (q, p) := \left(\sum_{i=0}^{\infty} \frac{\alpha_i}{n^{i+1}}, \quad \sum_{i=0}^{\infty} \frac{\alpha_{-(i+1)}}{n^{i+1}} \right), \tag{4}$$

which is bijective on a subset of Z_n with full (Lebesgue) measure [46]. Thus, J_n conjugates the symbolic shift with the baker map, $B_n = J_n \circ S \circ J_n^{-1}$, and they have equivalent dynamics.

The symbolic space allows to define a partition of the torus in terms of rectangles on phase space by finite sequences $\boldsymbol{\alpha}_{m_p,m_q} = \{\alpha_i\}_{i=-m_p}^{m_q-1}$ of length $m_p + m_q$, see illustration in figure 1(b). For such a finite sequence a subset of Z_n is defined as

$$[\boldsymbol{\alpha}_{m_p,m_q}] := \{\boldsymbol{\beta} \in Z_n : \beta_i = \alpha_i \ \forall \ -m_p \leqslant i \leqslant m_q - 1\}, \tag{5}$$

which contains all infinite sequences with the central part being equal to $\boldsymbol{\alpha}_{m_p,m_q}$. By construction $J_n([\boldsymbol{\alpha}_{m_p,m_q}])$ is a rectangle on $\mathbb{T}$ and a subset of A_{α_0}. There are $n^{m_p+m_q}$ such non-overlapping rectangles of size $\Delta p = 1/n^{m_p}$ and $\Delta q = 1/n^{m_q}$, see figure 1(b). In the following we will use the term rectangle for both, the sets of symbolic sequences $[\boldsymbol{\alpha}_{m_p,m_q}]$ and their image $J_n([\boldsymbol{\alpha}_{m_p,m_q}])$ on phase space.

3. Randomized quantum baker map with escape

In this section we first give the standard quantization of the baker map with escape. Then we introduce a randomization operator that acts locally on all phase-space rectangles, described by finite symbolic sequences, as introduced in section 2.2. The resonance states of this randomized baker map are multifractal down to the scale of randomization and uniformly fluctuating on smaller scales. Thus, the proposed randomization separates the smallest classical scale from the scale of a Planck cell. This allows for a well-defined semiclassical limit, where the size of a Planck cell becomes arbitrarily small compared to all classical scales.

3.1. Quantum baker map with escape

The baker map can be quantized with geometric quantization [73, 74]. For this the Hilbert space $\mathbb{C}^N$ with dimension $N \in n\mathbb{N}$ is considered and the time-evolution operator on $\mathbb{C}^N$ is defined in position basis as

$$\mathcal{B}_n := \mathcal{F}_N^{-1}\,\mathrm{diag}(\mathcal{F}_{N/n},\ldots,\mathcal{F}_{N/n}). \tag{6}$$

Here, the matrices $\mathcal{F}_M$ denote the discrete Fourier transform, which for arbitrary M are given by

$$(\mathcal{F}_M)_{ml} := M^{-\frac{1}{2}}\,\mathrm{e}^{-\frac{2\pi\mathrm{i}}{M}\left(m+\frac{1}{2}\right)\left(l+\frac{1}{2}\right)}. \tag{7}$$

Note that the exponents in the definition of $\mathcal{F}$ ensure for the closed baker map that symmetries of B_n are respected by the eigenfunctions of $\mathcal{B}_n$ [74].

The quantization of the baker map with escape is composed of the closed quantum map $\mathcal{B}_n$ and a reflectivity operator $\mathcal{R}_{\boldsymbol{r}}$. For constant escape from the rectangles A_k, as in the classical map, one has

$$\mathcal{R}_{\boldsymbol{r}} := \mathrm{diag}(\sqrt{r_0}\mathbb{1}_{N/n},\ldots,\sqrt{r_{n-1}}\mathbb{1}_{N/n}). \tag{8}$$

The quantization of the baker map with escape, equation (2), is then given by

$$\mathcal{B}_{n,\boldsymbol{r}} := \mathcal{B}_n\mathcal{R}_{\boldsymbol{r}}, \tag{9}$$

which has been extensively studied for full and partial escape [37, 45–48, 51].

3.2. Randomization

We introduce a procedure to randomize the quantum dynamics of the n-baker map. As randomization regions we consider the rectangles $[\boldsymbol{\alpha}_{\ell_p,\ell_q}]$ from a finite symbolic sequence of length ℓ_p in backward and ℓ_q in forward direction, see equation (5). The randomization within each of these $n^{\ell_p+\ell_q}$ rectangles is quantum mechanically achieved with random matrices $\mathcal{M}_{N_{\mathrm{CUE}}}$ of dimension N_{CUE}, where we choose the circular unitary ensemble (CUE) which has no symmetries. Then the dimension N of the full Hilbert space is given by $N = n^{\ell_q+\ell_p}N_{\mathrm{CUE}}$. The randomization operator in a basis corresponding to these rectangles is given by the block-diagonal operator

$$\hat{\mathcal{U}}^{\mathrm{CUE}}_{\ell_p,\ell_q} = \mathrm{diag}(\mathcal{M}_{N_{\mathrm{CUE}}},\ldots,\mathcal{M}_{N_{\mathrm{CUE}}}), \tag{10}$$

consisting of $n^{\ell_q+\ell_p}$ CUE-matrices with dimension N_{CUE}. In order to represent this operator in position basis we define a block matrix of n^{ℓ_q} Fourier transformations,

$$\mathcal{U}_{\ell_q} = \mathrm{diag}(\mathcal{F}_{N/n^{\ell_q}}, \ldots, \mathcal{F}_{N/n^{\ell_q}}), \tag{11}$$

acting on vertical phase-space regions that consist each of n^{ℓ_p} randomization regions. The randomization operator in position basis is then given by

$$\mathcal{U}^{\mathrm{CUE}}_{\ell_p,\ell_q} = {\mathcal{U}_{\ell_q}}^{-1}\, \hat{\mathcal{U}}^{\mathrm{CUE}}_{\ell_p,\ell_q}\, \mathcal{U}_{\ell_q}. \tag{12}$$

Altogether, we define the randomized baker map with escape as the composition of randomization, escape and baker map,

$$\mathcal{B}_{n,\boldsymbol{r},\ell_p,\ell_q} := \mathcal{B}_n\, \mathcal{R}_{\boldsymbol{r}}\, \mathcal{U}^{\mathrm{CUE}}_{\ell_p,\ell_q}. \tag{13}$$

3.3. Resonance states

Right resonance states of the randomized baker map with escape are defined by

$$\mathcal{B}_{n,\boldsymbol{r},\ell_p,\ell_q}\ \psi = \mathrm{e}^{\mathrm{i}\theta-\gamma/2}\ \psi, \tag{14}$$

where γ is the decay rate, i.e., the square of the norm of ψ decays by a factor of $\mathrm{e}^{-\gamma}$ when $\mathcal{B}_{n,\boldsymbol{r},\ell_p,\ell_q}$ is applied. The phase θ and decay rate γ are related to the energy and width of resonance poles in autonomous scattering [75, 76]. The corresponding left resonance states are not discussed separately, as one can show that they are right resonance states for the related operator, where $\mathcal{R}_{\boldsymbol{r}}$ is replaced with ${\mathcal{R}_{\boldsymbol{r}}}^{-1}$ in equation (13), i.e., with inverted reflectivity constants, $1/r_k$.

As we are interested in the phase-space distribution of resonance states ψ, we consider the Husimi function $\mathcal{H}_\psi$ [12, 77] which is a smooth probability density. It is defined using the overlap of the state ψ with a coherent state $c(q, p)$ centered at some phase-space point (q, p),

$$\mathcal{H}_\psi(q, p) = N\|\langle c(q, p)|\psi\rangle\|^2, \tag{15}$$

where N is the Hilbert space dimension. For quantum maps on the torus the coherent states are defined in reference [12]. In the following numerical illustrations the width of the coherent states is chosen to be symmetric in phase space.

We illustrate in figure 2(a) in the left panel a resonance state for the randomized three-baker map with $n = 3$ stripes, reflectivities $\boldsymbol{r} = (0.2, 0.01, 1)$ and $N = 35 \times 3^6 = 25\,515$ with decay rate closest to γ_{typ}. Here the randomization regions are defined by $(\ell_p, \ell_q) = (0, 1)$, i.e., they correspond to the rectangles A_k. One observes that the resonance state is not uniformly fluctuating in each of the $n = 3$ randomization regions. Instead, we find a finer substructure, where each randomization region has $n = 3$ subregions in p-direction, leading to a 3×3 grid. This subregion structure is discussed in more detail in appendix A.

Within each subregion the resonance state visually fluctuates as in closed chaotic quantum maps and we find an exponential distribution around the average, as conjectured in reference [56] for quantum maps with escape. The subregion structure remains the same for increasing N and the Planck cell becomes arbitrarily small compared to it, giving a well-defined semi-classical limit. This is in contrast to deterministic quantum maps with escape, where even for arbitrarily large N the phase-space structure of a resonance state is multifractal down to the scale of a Planck cell.

In figures 2(b) and (c) the randomization regions are defined on finer scales by $(\ell_p, \ell_q) = (1, 2)$ and $(\ell_p, \ell_q) = (2, 3)$, respectively. The resonance states (left panel) are again uniformly

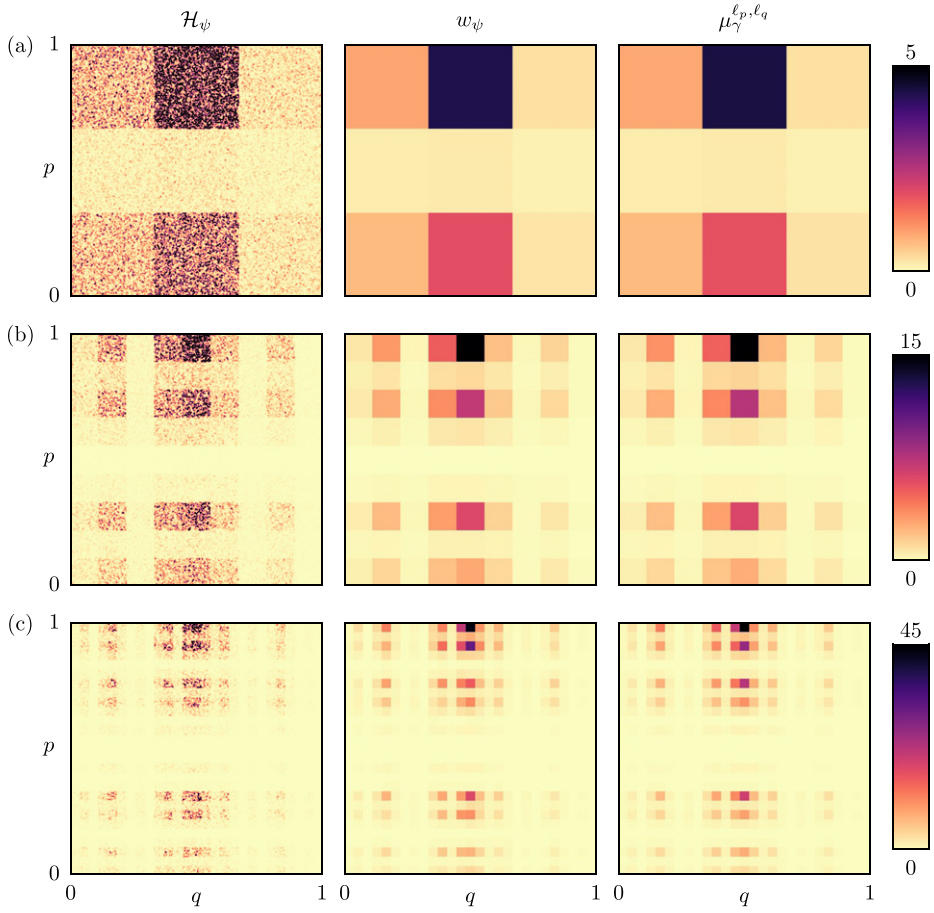

Figure 2. Phase-space distributions of resonance states and classical measures for randomization regions on increasingly finer levels (a) $(\ell_p, \ell_q) = (0, 1)$, (b) $(\ell_p, \ell_q) = (1, 2)$, and (c) $(\ell_p, \ell_q) = (2, 3)$ for the randomized three-baker map with $\boldsymbol{r} = (0.2, 0.01, 1)$. Shown is (left) Husimi function $\mathcal{H}_\psi$ for the resonance state ψ with decay rate γ closest to γ_{typ} for $N = 25\,515$, (middle) projected weights $w_\psi([\boldsymbol{\alpha}_{\ell_p+1,\ell_q}])$ on the level of the randomization subregions, and (right) corresponding classical measure $\mu_\gamma^{\ell_p,\ell_q}$ derived in section 4.

fluctuating on n subregions of each randomization region, leading to a $n^{\ell_p+1} \times n^{\ell_q}$-grid structure. Again, for increasing N the Planck cell size becomes arbitrarily small compared to the phase-space structures of resonance states.

For increasingly finer randomization levels we observe in figures 2(a)–(c) that the phase-space structure on smaller scales resembles (qualitatively) the phase-space structure on larger scales. For example the region $(q, p) \in [1/3, 2/3] \times [2/3, 1]$ in figure 2(b) looks similar to the full phase space in figure 2(a). In the limit of $\ell_p, \ell_q \to \infty$ with sufficiently large N this leads to multifractal structures.

Note as an aside, that if for a fixed Hilbert space dimension N, the number $n^{\ell_p+\ell_q}$ of randomization regions is increased, the dimension $N_{\text{CUE}} = N/n^{\ell_p+\ell_q}$ of the random matrices becomes smaller as well as the number of Planck cells $N_{\text{sub}} = N_{\text{CUE}}/n = N/n^{\ell_p+1+\ell_q}$ within each randomization subregion. In figures 2(a)–(c) this leads to $N_{\text{sub}} = 2835$, $N_{\text{sub}} = 315$, and

$N_{\rm sub} = 35$, respectively. Numerically, this limits the number of levels that can be explored, while still having $N_{\rm sub} \gg 1$.

3.4. Weight of resonance state on rectangular phase-space regions

In order to compare the phase-space structure of a resonance state with some classical measure, we choose rectangular phase-space regions onto which we project the resonance state. A suitable projector is defined by first projecting the position representation to the interval corresponding to the extent of the rectangle in q-direction. The second step is a transformation to the momentum representation and projection on the interval corresponding to the extent of the rectangle in p-direction. For convenience we use the rectangles $[\boldsymbol{\alpha}_{m_p,m_q}]$ partitioning the phase space based on the finite symbolic sequences of the baker map. We define a projector $P_{[m_p,m_q]}$ for all $n^{m_p+m_q}$ possible finite sequences $\boldsymbol{\alpha}_{m_p,m_q}$ with $\alpha_i \in \{0,\ldots,n-1\}$,

$$P_{[\boldsymbol{\alpha}_{m_p,m_q}]} = \mathcal{U}_{m_q}{}^{-1}\ \mathrm{diag}(\underbrace{\mathbb{O}_{N_{\rm rect}},\ldots,\mathbb{O}_{N_{\rm rect}}}_{I(\boldsymbol{\alpha}_{m_p,m_q})},\mathbb{1}_{N_{\rm rect}},\underbrace{\mathbb{O}_{N_{\rm rect}},\ldots,\mathbb{O}_{N_{\rm rect}}}_{n^{m_p+m_q}-I(\boldsymbol{\alpha}_{m_p,m_q})-1})\ \mathcal{U}_{m_q}, \quad (16)$$

where $N_{\rm rect}$ is the dimension of the Hilbert space of each rectangle and $N = n^{m_p+m_q}N_{\rm rect}$ the total Hilbert space dimension. Here the rectangles $[\boldsymbol{\alpha}_{m_p,m_q}]$ are ordered according to the index $I(\boldsymbol{\alpha}_{m_p,m_q}) = \sum_{i=0}^{m_p-1}\alpha_{i-m_p}n^i + n^{m_p}\sum_{i=0}^{m_q-1}\alpha_{m_q-1-i}n^i$, which counts the rectangles first in the leftmost column from bottom to top, then in the second column, and so on. The projected weight of a state ψ on a rectangle $[\boldsymbol{\alpha}_{m_p,m_q}]$ is then given by

$$w_\psi([\boldsymbol{\alpha}_{m_p,m_q}]) = \|P_{[\boldsymbol{\alpha}_{m_p,m_q}]}\psi\|^2. \quad (17)$$

Alternatively, one may determine the weights by integrating the Husimi function over the corresponding rectangle on $\mathbb{T}$, $w_\psi([\boldsymbol{\alpha}_{m_p,m_q}]) = \int_{J_n([\boldsymbol{\alpha}_{m_p,m_q}])}\mathcal{H}_\psi(q,p)\mathrm{d}\mu_{\rm L}$. Note that the weights of both approaches agree in the semiclassical limit $N\to\infty$. Convergence is slower when using the Husimi function, as the weight in rectangles with small weights is strongly influenced by neighboring rectangles with large weights due to the finite resolution of the Husimi function.

In figures 2(a)–(c) in the middle panel the weight on all subregion rectangles $[\boldsymbol{\alpha}_{\ell_p+1,\ell_q}]$ of a resonance state is illustrated. This can be compared to classical measures in the right panel, derived in section 4, showing excellent agreement on a qualitative level. A quantitative comparison will be presented in section 5.

We emphasize that while figure 2 shows results for just one exemplary decay rate $\gamma_{\rm typ}$, the weight in each subregion rectangle depends on the decay rate γ. It is the goal of this paper to derive classical measures for arbitrary decay rates. In the next section we consider randomization regions with arbitrary but fixed ℓ_p and ℓ_q and make a conjecture for the semiclassical limit $N\to\infty$.

4. Semiclassical structure of resonance states

In this section we present a conjecture for the semiclassical structure of resonance states of the randomized baker map with partial escape. To this end we introduce classical measures, which (i) are conditionally invariant with some desired decay rate γ on scales larger than the scale of randomization and (ii) obey an extremum principle derived from a local random vector model in each randomization region.

4.1. Conditional invariance on rectangles

Semiclassically, resonance states of quantum maps with escape converge to conditionally invariant measures of the same decay rate [45, 46, 53]. A measure μ on $\mathbb{T}$ is conditionally invariant [57] with respect to the classical baker map B_n with escape r, if there exists a decay rate $\gamma \in \mathbb{R}$ with

$$\int_{B_n^{-1}(A)} r \, \mathrm{d}\mu = \mathrm{e}^{-\gamma} \, \mu(A) \quad \forall \, A \subset \mathbb{T}. \tag{18}$$

For constant reflectivity factors r_k from the rectangles A_k, as considered in this paper, this condition simplifies for subsets of A_k to

$$r_k \, \mu(C) = \mathrm{e}^{-\gamma} \, \mu(B_n(C)) \quad \forall \, C \subset A_k. \tag{19}$$

In general, equation (18) holds for all measurable sets $A \subset \mathbb{T}$ up to arbitrary small scales, which is related to the multifractal structure of conditionally invariant measures. However, for the randomized quantum baker map, as introduced in the last section, we observe no structure of resonance states on scales finer than the subregions of the randomization regions $[\boldsymbol{\alpha}_{\ell_p,\ell_q}]$, see figures 2(a)–(c) left panel. For this reason, conditional invariance cannot be satisfied on arbitrarily fine scales. This motivates to introduce the following scale dependent definition. We call a measure μ on $\mathbb{T}$ conditionally invariant down to the scale (ℓ_p, ℓ_q) with respect to the baker map with escape $B_{n,\boldsymbol{r}}$, if equation (19) holds for all sets $C = J_n([\boldsymbol{\alpha}_{\ell_p,\ell_q}])$.

We assume for the randomized quantum baker map, that the resonance states converge in the semiclassical limit to measures which satisfy conditional invariance down to the scale (ℓ_p, ℓ_q) of the randomization regions and are constant on the subregions of scale $(\ell_p + 1, \ell_q)$. Such measures are shown in figures 2(a)–(c) right panel and are derived in this section.

From conditional invariance down to the scale of randomization we derive constraints for μ. Recall that the randomization regions are defined as the rectangles $[\boldsymbol{\alpha}_{\ell_p,\ell_q}] = [\alpha_{-\ell_p} \ldots \alpha_{-1} \cdot \alpha_0 \alpha_1 \ldots \alpha_{\ell_q-1}]$ with $\alpha_i \in \{0, \ldots, n-1\}$ for all $-\ell_p \leqslant i \leqslant \ell_q - 1$. Their iterates are given by $[S(\boldsymbol{\alpha}_{\ell_p,\ell_q})] = [\alpha_{-\ell_p} \ldots \alpha_{-1}\alpha_0 \cdot \alpha_1 \ldots \alpha_{\ell_q-1}]$. These iterates correspond to rectangles, which are stretched by a factor n in q-direction and compressed by $1/n$ in p-direction. Each of these iterates overlaps with exactly n of the randomization regions (and vice versa), see illustration in figure 1(b). Hence, the original and the iterated randomization rectangles can be partitioned as follows,

$$[\boldsymbol{\alpha}_{\ell_p,\ell_q}] = \bigcup_{j=0}^{n-1} [j\boldsymbol{\alpha}_{\ell_p,\ell_q}], \qquad [S(\boldsymbol{\alpha}_{\ell_p,\ell_q})] = \bigcup_{j=0}^{n-1} [S(\boldsymbol{\alpha}_{\ell_p,\ell_q})j], \tag{20}$$

where for each $j \in \{0, \ldots, n-1\}$ the smaller rectangles $[j\boldsymbol{\alpha}_{\ell_p,\ell_q}] := [j\,\alpha_{-\ell_p} \ldots \alpha_{-1} \cdot \alpha_0 \alpha_1 \ldots \alpha_{\ell_q-1}]$ and $[S(\boldsymbol{\alpha}_{\ell_p,\ell_q})j] := [\alpha_{-\ell_p} \ldots \alpha_0 \cdot \alpha_1 \alpha_2 \ldots \alpha_{\ell_q-1}\, j]$ are the subregions of the randomization regions on which the measure μ is constant.

Conditional invariance down to the scale of the randomization regions $[\boldsymbol{\alpha}_{\ell_p,\ell_q}]$ implies, by setting $C = J_n([\boldsymbol{\alpha}_{\ell_p,\ell_q}])$ in equation (19) with $C \subset A_{\alpha_0}$, that

$$r_{\alpha_0} \, \mu([\boldsymbol{\alpha}_{\ell_p,\ell_q}]) = \mathrm{e}^{-\gamma} \, \mu([S(\boldsymbol{\alpha}_{\ell_p,\ell_q})]) \tag{21}$$

for all multi-indices $\boldsymbol{\alpha}_{\ell_p,\ell_q}$. Inserting the partitions from equation (20) we get

$$r_{\alpha_0}\,\mu\left(\bigcup_{j=0}^{n-1}[j\boldsymbol{\alpha}_{\ell_p,\ell_q}]\right)=\mathrm{e}^{-\gamma}\,\mu\left(\bigcup_{j=0}^{n-1}[S(\boldsymbol{\alpha}_{\ell_p,\ell_q})j]\right). \tag{22}$$

This gives the constraints of conditional invariance on the weights of all subregion rectangles with scales (ℓ_p+1,ℓ_q),

$$r_{\alpha_0}\sum_{j=0}^{n-1}\mu([j\boldsymbol{\alpha}_{\ell_p,\ell_q}])=\mathrm{e}^{-\gamma}\sum_{j=0}^{n-1}\mu([S(\boldsymbol{\alpha}_{\ell_p,\ell_q})j]), \tag{23}$$

holding for all possible finite symbolic sequences of the form $\boldsymbol{\alpha}_{\ell_p,\ell_q}=\alpha_{-\ell_p}\ldots\alpha_{-1}.\alpha_0\ldots\alpha_{\ell_q-1}$ with $\alpha_i\in\{0,\ldots,n-1\}$. Altogether, these are $n^{\ell_p+\ell_q}$ constraints on the subregion weights.

Normalization of the measure μ

$$\mu(\mathbb{T})=\mu\left(\bigcup_{j=0}^{n-1}\bigcup_{\alpha_{-\ell_p}=0}^{n-1}\ldots\bigcup_{\alpha_0=0}^{n-1}\ldots\bigcup_{\alpha_{\ell_q-1}=0}^{n-1}[j\boldsymbol{\alpha}_{\ell_p,\ell_q}]\right)=1 \tag{24}$$

adds one more constraint

$$\sum_{j=0}^{n-1}\sum_{\alpha_{-\ell_p}=0}^{n-1}\ldots\sum_{\alpha_0=0}^{n-1}\ldots\sum_{\alpha_{\ell_q-1}=0}^{n-1}\mu([j\boldsymbol{\alpha}_{\ell_p,\ell_q}])=1. \tag{25}$$

Thus, conditional invariance down to scale (ℓ_p,ℓ_q), equation (23), and normalization, equation (25), give $n^{\ell_p+\ell_q}+1$ constraints on the weights of all $n^{\ell_p+1+\ell_q}$ subregion rectangles. This leads to the question, how quantum mechanics distributes the weight over the subregion rectangles under the restrictions of equations (23) and (25). This will be answered in the next section.

4.2. Local random vector model

Based on a random vector model [12, 24] that is applied locally in every randomization region, we derive in the following the semiclassical structure of resonance states of the randomized quantum baker map and its dependence on the decay rate γ. We introduce the local random vector model for each randomization region as follows. Let $[\boldsymbol{\alpha}_{\ell_p,\ell_q}]$ be one of these randomization regions with N_{CUE} sites, corresponding to the number of Planck cells in this randomization region. Let site weight factors $f_i\geqslant 0$ with $\sum_{i=0}^{N_{\mathrm{CUE}}-1}f_i=1$ describe how the *a priori* unknown weight $\mu([\boldsymbol{\alpha}_{\ell_p,\ell_q}])$ of the randomization region is distributed on its sites, such that the weight at site i is given by $f_i\,\mu([\boldsymbol{\alpha}_{\ell_p,\ell_q}])$. Let these site weight factors f_i be given by the intensities $f_i=|c_i|^2$ of a random vector with complex amplitudes $c_i\in\mathbb{C}$, which must be normalized $\sum_{i=0}^{N_{\mathrm{CUE}}-1}|c_i|^2=1$, following the definition of the factors f_i.

For such normalized random vectors of dimension N_{CUE} the joint probability distribution of its complex amplitudes is given by [18, 78],

$$P(\{c_i\})=\frac{\Gamma(N_{\mathrm{CUE}})}{\pi^{N_{\mathrm{CUE}}}}\,\delta\left(\sum_{i=0}^{N_{\mathrm{CUE}}-1}|c_i|^2-1\right). \tag{26}$$

By integration over the angle of each complex amplitude it follows that its intensities, i.e., the site weight factors $f_i = |c_i|^2$, have the joint probability distribution

$$P(\{f_i\}) = \Gamma(N_{\mathrm{CUE}})\,\delta\left(\sum_{i=0}^{N_{\mathrm{CUE}}-1} f_i - 1\right), \tag{27}$$

which is uniform for normalized factors f_i. This uniformity will be used below. In the special case that the randomization region is the entire phase space $\mathbb{T}$, which has measure $\mu(\mathbb{T}) = 1$, this is equivalent to the usual random vector model for chaotic maps [12, 24].

Each randomization region consists of n subregions $[j\boldsymbol{\alpha}_{\ell_p,\ell_q}]$ with $j \in \{0,\ldots,n-1\}$, where each subregion has N_{sub} sites if $N_{\mathrm{CUE}} = nN_{\mathrm{sub}}$ is chosen appropriately. We define a subregion weight factor F_j by the relative weight of the set $[j\boldsymbol{\alpha}_{\ell_p,\ell_q}]$ to $[\boldsymbol{\alpha}_{\ell_p,\ell_q}]$,

$$F_j = \frac{\mu([j\boldsymbol{\alpha}_{\ell_p,\ell_q}])}{\mu([\boldsymbol{\alpha}_{\ell_p,\ell_q}])}. \tag{28}$$

The F_j are thus given by the sum over all corresponding site weight factors f_i. For a suitable ordering of the f_i this can be expressed as

$$F_j = \sum_{i=0}^{N_{\mathrm{sub}}-1} f_{jN_{\mathrm{sub}}+i} \quad \forall\ j = 0,\ldots,n-1. \tag{29}$$

Note that normalization of the subregion weight factors, $\sum_{j=0}^{n-1} F_j = \sum_{i=0}^{N_{\mathrm{CUE}}-1} f_i = 1$, follows from the above normalization of the site weight factors f_i.

The joint probability distribution $P(\{F_j\})$ of subregion weight factors in a randomization region is given by integrating over the uniform joint probability distribution of site weight factors, equation (27), while fulfilling equation (29) for all j,

$$\begin{aligned} P(\{F_j\}) &= \int \prod_{j=0}^{n-1} \delta\left(F_j - \sum_{i=0}^{N_{\mathrm{sub}}-1} f_{jN_{\mathrm{sub}}+i}\right)\, \mathrm{d}P(\{f_i\}) \\ &= \Gamma(N_{\mathrm{CUE}})\,\delta\left(\sum_{j=0}^{n-1} F_j - 1\right) \prod_{j=0}^{n-1} \int \delta \\ &\quad \times \left(F_j - \sum_{i=0}^{N_{\mathrm{sub}}-1} f_{jN_{\mathrm{sub}}+i}\right) \prod_{i=0}^{N_{\mathrm{sub}}-1} \mathrm{d}f_{jN_{\mathrm{sub}}+i}. \end{aligned} \tag{30}$$

Here for each j the integral gives the volume of an $(N_{\mathrm{sub}}-1)$-dimensional standard simplex within the N_{sub}-dimensional space $\{f_{jN_{\mathrm{sub}}}, f_{jN_{\mathrm{sub}}+1}, \ldots, f_{jN_{\mathrm{sub}}+N_{\mathrm{sub}}-1}\}$, which is scaled in all dimensions with the factor F_j and thus is proportional to $F_j^{N_{\mathrm{sub}}-1}$. For example, for $N_{\mathrm{sub}} = 3$ it is a triangle in the 3D space $(f_{3j}, f_{3j+1}, f_{3j+2})$ with corners $(F_j, 0, 0)$, $(0, F_j, 0)$, $(0, 0, F_j)$ and 2D volume proportional to F_j^2. Thus we obtain for the joint probability distribution of normalized subregion weight factors,

$$P(\{F_j\}) \propto \prod_{j=0}^{n-1} F_j^{N_{\mathrm{sub}}-1}. \tag{31}$$

We now extend this argument to all $n^{\ell_p+\ell_q}$ randomization regions $[\boldsymbol{\alpha}_{\ell_p,\ell_q}]$, each with n subregion weight factors $F_{j\boldsymbol{\alpha}_{\ell_p,\ell_q}}$ from the local random vector model. Assuming independence, the joint probability distribution of all subregion weight factors is proportional to

$$P(\{F_{j\boldsymbol{\alpha}_{\ell_p,\ell_q}}\}) \propto \prod_{\boldsymbol{\alpha}_{\ell_p,\ell_q}} \prod_{j=0}^{n-1} F_{j\boldsymbol{\alpha}_{\ell_p,\ell_q}}^{N_{\mathrm{sub}}-1} = \left(\prod_{\boldsymbol{\alpha}_{\ell_p,\ell_q}} \prod_{j=0}^{n-1} F_{j\boldsymbol{\alpha}_{\ell_p,\ell_q}} \right)^{N_{\mathrm{sub}}-1}. \tag{32}$$

In the semiclassical limit, $N_{\mathrm{sub}} \to \infty$, this distribution approaches a delta function at the maximum of the product of the subregion weight factors, $\prod_{\boldsymbol{\alpha}_{\ell_p,\ell_q}} \prod_{j=0}^{n-1} F_{j\boldsymbol{\alpha}_{\ell_p,\ell_q}}$. In this product we insert the definition of the subregion weight factors, equation (28),

$$F_{j\boldsymbol{\alpha}_{\ell_p,\ell_q}} = \frac{\mu([j\boldsymbol{\alpha}_{\ell_p,\ell_q}])}{\sum_{l=0}^{n-1} \mu([l\boldsymbol{\alpha}_{\ell_p,\ell_q}])}, \tag{33}$$

using the subregion weights $\mu([j\boldsymbol{\alpha}_{\ell_p,\ell_q}])$ and the weight of the corresponding randomization region $\mu([\boldsymbol{\alpha}_{\ell_p,\ell_q}]) = \sum_{l=0}^{n-1} \mu([l\boldsymbol{\alpha}_{\ell_p,\ell_q}])$. This allows for writing the product of subregion weight factors as a product of relative weights,

$$\Pi(\mu) = \prod_{\boldsymbol{\alpha}_{\ell_p,\ell_q}} \prod_{j=0}^{n-1} \frac{\mu([j\boldsymbol{\alpha}_{\ell_p,\ell_q}])}{\sum_{l=0}^{n-1} \mu([l\boldsymbol{\alpha}_{\ell_p,\ell_q}])}. \tag{34}$$

Thus the local random vector model for each randomization region leads to the following extremum principle: the subregion weights $\mu([j\boldsymbol{\alpha}_{\ell_p,\ell_q}])$ maximize the product $\Pi(\mu)$ of relative weights, equation (34), under the constraints of conditional invariance, equation (23), and normalization, equation (25). They can be determined, e.g., by using the method of Lagrange multipliers leading to a set of coupled nonlinear equations. These subregion weights $\mu([j\boldsymbol{\alpha}_{\ell_p,\ell_q}])$ define a classical measure $\mu_\gamma^{\ell_p,\ell_q}$ on $\mathbb{T}$, that is conditionally invariant down to the scale of the randomization regions, determined by ℓ_p and ℓ_q, and that depends on the decay rate γ.

In figures 2(a)–(c) in the right panel examples of such classical measures $\mu_\gamma^{\ell_p,\ell_q}$ for three increasing levels of randomization $\ell_p \in \{0,1,2\}$ with $\ell_q = \ell_p + 1$ are shown. We find quite good agreement with the structure of the resonance states (left panel) and the projected weights within each subregion rectangle (middle panel). Slight deviations are observable in (c), where the subregion dimension $N_{\mathrm{sub}} = 35$ is quite small and the projected weights are still influenced by the fluctuations of an individual resonance state.

4.3. Semiclassical conjecture

The following conjecture is formulated in analogy to quantum ergodicity in closed chaotic maps [12, 79]. For fixed ℓ_p and ℓ_q we conjecture that the classical measures $\mu_\gamma^{\ell_p,\ell_q}$ are the semiclassical limit measures of resonance states ψ of the randomized quantum baker map with escape $\mathcal{B}_{n,\boldsymbol{r},\ell_p,\ell_q}$, which decay with the rate γ. In particular, let $\{\mathcal{B}^N_{n,\boldsymbol{r},\ell_p,\ell_q}\}$ be the ensemble of randomized quantum baker maps with dimension N. Let ψ_N be an eigenstate of any member $\mathcal{B}^N_{n,\boldsymbol{r},\ell_p,\ell_q}$ of the ensemble, $\mathcal{B}^N_{n,\boldsymbol{r},\ell_p,\ell_q}\psi_N = \lambda_N \psi_N$. For a sequence of such states with decay rates $\gamma_N = -\ln|\lambda_N|^2 \overset{N\to\infty}{\to} \gamma$, and for all observables a on $\mathbb{T}$ with quantization $\mathrm{op}_N(a)$ we expect

$$\langle\psi_N|\mathrm{op}_N(a)|\psi_N\rangle \overset{N\to\infty}{\to} \mu_\gamma^{\ell_p,\ell_q}(a) = \int_{\mathbb{T}} a \,\mathrm{d}\mu_\gamma^{\ell_p,\ell_q}. \tag{35}$$

This means, that the quantum expectation values converge to the classical ones given by $\mu_\gamma^{\ell_p,\ell_q}$. Note that there are exceptional sequences ψ_N from exceptional members of the ensemble $\{\mathcal{B}^N_{n,\boldsymbol{r},\ell_p,\ell_q}\}$, such that convergence in equation (35) is expected just for a suitable subsequence of density one. A quantitative analysis of the quantum–classical agreement is given in section 5.

4.4. Properties of the classical measure $\mu_\gamma^{\ell_p,\ell_q}$

We list some relevant properties and remarks on the classical measures $\mu_\gamma^{\ell_p,\ell_q}$:

(a) Numerics for increasing ℓ_p, ℓ_q suggests that in the limit $\ell_p, \ell_q \to \infty$ the classical measures $\mu_\gamma^{\ell_p,\ell_q}$ converge weakly to some limiting measure μ_γ^*, see appendix B.

(b) The product $\Pi(\mu)$ of relative weights, equation (34), is maximal if all relative weights are equally given by $1/n$. Assuming conditional invariance one can show that this implies that the measures are also uniform within the sets $[\boldsymbol{\alpha}_{0,\ell_q}]$, i.e., along the p-direction. The subregion weights follow as $\mu([\boldsymbol{\alpha}_{\ell_p+1,\ell_q}]) = \prod_{i=0}^{\ell_q-1} r_{\alpha_i}^{-1}/\mathcal{N}$ with some normalization $\mathcal{N}$. This measure is conditionally invariant with decay rate γ_{inv}, the natural growth rate of the inverse map, see section 2.1.

(c) For the natural decay rate γ_{nat} one needs to rewrite the product $\Pi(\mu)$ using conditional invariance, equation (23), with decay rate γ_{nat}, leading after reordering to

$$\Pi(\mu) = \prod_{\boldsymbol{\alpha}_{\ell_p,\ell_q}} \prod_{j=0}^{n-1} r_{\alpha_{-1}}\, \mathrm{e}^{\gamma_{\text{nat}}} \frac{\mu([\boldsymbol{\alpha}_{\ell_p,\ell_q} j])}{\sum_{l=0}^{n-1} \mu([\boldsymbol{\alpha}_{\ell_p,\ell_q} l])}. \tag{36}$$

This product is maximal if all relative weights, now with respect to iterated randomization regions, are equally given by $1/n$. One can show that this implies that all subregion weights are given by $\mu([\boldsymbol{\alpha}_{\ell_p+1,\ell_q}]) = \prod_{i=-1}^{-\ell_p-1} r_{\alpha_i}/\mathcal{N}$ with some normalization $\mathcal{N}$, i.e., the measure is uniform in q-direction. This measure is indeed conditionally invariant with decay rate γ_{nat}.

(d) The classical measure $\mu_\gamma^{\ell_p,\ell_q}$ for the special case γ_{nat} (γ_{inv}) is consistent with the general observation that at the (inverse) natural decay rate resonance states are uniform along the unstable (stable) direction [25, 54].

(e) We mention as an aside, that if one applies this extremum principle to closed chaotic systems, it leads to the uniform distribution, which is consistent with quantum ergodicity [10–12].

(f) It is possible to apply the local random vector model combined with conditional invariance to random matrices with partial escape, consistently retrieving the results of reference [56, appendix D]. The details are given in appendix C.

(g) If simultaneously decreasing the scale of the randomization regions and increasing N, such that still $N_{\text{sub}} \to \infty$ holds, we expect that the local random vector model leads to the same limiting measures μ_γ^*, as discussed in remark (a) above.

5. Numerical verification

In this section we present quantitative numerical support for the semiclassical conjecture given in the last section, going beyond the qualitative comparison of figure 2. All results are presented for single realizations of the randomized quantum baker map without averaging.

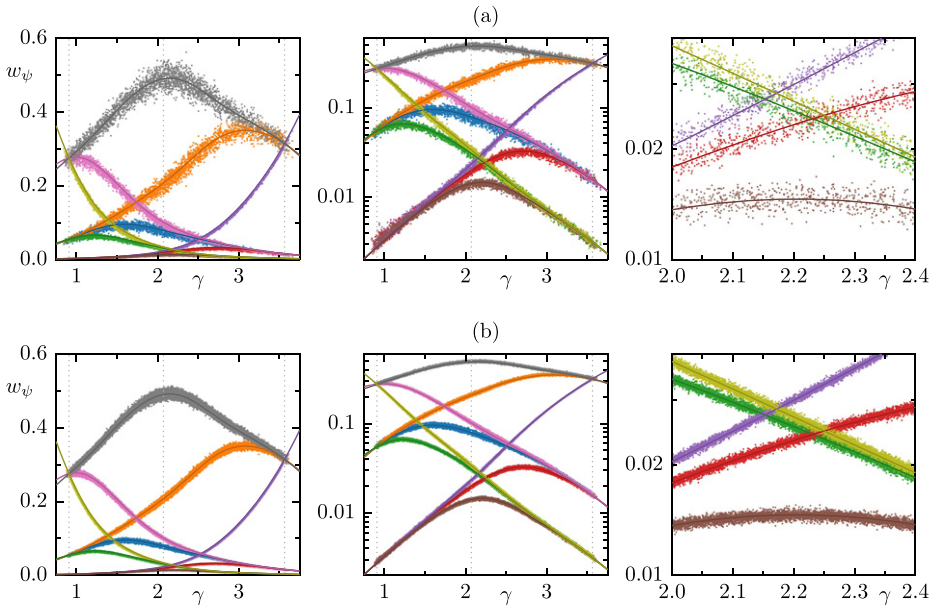

Figure 3. Comparison of the nine projected weights $w_{\psi_i}([\boldsymbol{\alpha}_{1,1}])$ of each resonance state ψ_i vs its decay rate γ_i (dots) and classical measures $\mu_\gamma^{\ell_p,\ell_q}([\boldsymbol{\alpha}_{1,1}])$ (lines) for three-baker map with $\boldsymbol{r} = (0.2, 0.01, 1)$ and randomization level $(\ell_p, \ell_q) = (0, 1)$ for Hilbert space dimension (a) $N = 2835$ and (b) $N = 25\,515$. The same data is shown on linear (left) and logarithmic scale (middle) as well as a magnification (right). Decay rates γ_{nat}, γ_{typ}, and γ_{inv} are indicated (dotted lines).

5.1. Weights on classically large regions

In order to test the semiclassical conjecture, equation (35), we choose as observables the projection operators on classically large regions compared to a Planck cell. Specifically, we use squares given by symbolic sequences $[\boldsymbol{\alpha}_{\ell,\ell}]$ with $\ell = 1$ and $\ell = 2$. For different systems and Hilbert space dimensions we consider all resonance states ψ_i and show how the projected weights $w_{\psi_i}([\boldsymbol{\alpha}_{\ell,\ell}])$, equation (17), depend on their quantum decay rate γ_i. This is compared to the classical measures $\mu_\gamma^{\ell_p,\ell_q}([\boldsymbol{\alpha}_{\ell,\ell}])$ on these squares and their dependence on γ. The Hilbert space dimension N is in all cases chosen to be a multiple of the number $n^{\ell_p+1+\ell_q}$ of subregions.

In figure 3 we consider the three-baker map with $\boldsymbol{r} = (0.2, 0.01, 1)$ and randomization level $(\ell_p, \ell_q) = (0, 1)$ for increasing Hilbert space dimension. For $\ell = 1$ there are $n^{2\ell} = 9$ quantum and classical weights which are compared. We observe that the quantum weights (dots) scatter symmetrically around the classical measures (lines). The width of the distribution decreases with increasing Hilbert space dimension for each of the considered squares (compare (a) and (b)), supporting the semiclassical conjecture. This also holds for small weights, as can be seen on the logarithmic scale (middle panel).

At the natural decay rates γ_{nat} and γ_{inv} the measures are constant along one direction, see section 4.4, and several weights are identical in agreement with the properties of the resonance states.

Figure 4 shows the comparison for smaller randomization regions $(\ell_p, \ell_q) = (1, 2)$ and weights on smaller phase-space regions $[\boldsymbol{\alpha}_{\ell,\ell}]$ with $\ell = 2$. There are $n^{2\ell} = 81$ such regions out of which nine are presented in the figure, corresponding to the phase-space region

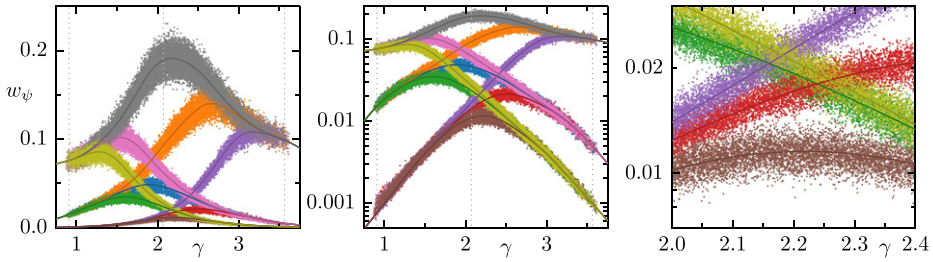

Figure 4. Same as figure 3(b), but for randomization level $(\ell_p, \ell_q) = (1, 2)$ and for nine selected squares from $[\boldsymbol{\alpha}_{2,2}]$ with symbolic sequence $\boldsymbol{\alpha} = i2 \cdot 1j$ and $i, j \in \{0, 1, 2\}$.

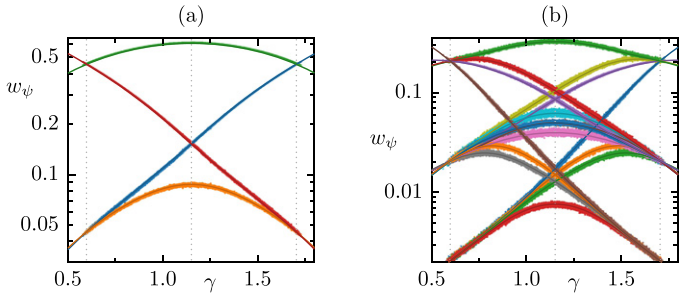

Figure 5. Comparison of $n^{2\ell}$ projected weights $w_{\psi_i}([\boldsymbol{\alpha}_{\ell,\ell}])$ of each resonance state ψ_i (dots) and classical measures $\mu_\gamma^{\ell_p,\ell_q}([\boldsymbol{\alpha}_{\ell,\ell}])$ (lines) for two-baker map with $\boldsymbol{r} = (0.1, 1)$ and randomization level $(\ell_p, \ell_q) = (\ell - 1, \ell)$ for (a) $\ell = 1$ and (b) $\ell = 2$ for Hilbert space dimension $N = 25\,600$. Decay rates γ_{nat}, γ_{typ}, and γ_{inv} are indicated (dotted lines).

$(q, p) \in [1/3, 2/3] \times [2/3, 1]$, see figure 2(a). Again, quantum and classical weights show excellent agreement. The width of each distribution is wider than in figure 3(b), as the observables are smaller phase-space regions. For larger Hilbert space dimension N it is expected to decrease. We emphasize that the dependence on γ qualitatively resembles the results for $(\ell_p, \ell_q) = (0, 1)$ shown in figure 3, but now on a smaller scale in phase space. This indicates again the multifractal phase-space structure, which emerges for smaller randomization regions, as observed in figure 2.

Additionally, we show the quantum–classical comparison for the two-baker map with $\boldsymbol{r} = (0.1, 1)$ for two randomization levels in figure 5. Again, we observe excellent agreement for all decay rates.

5.2. Jensen–Shannon divergence

In order to further analyze the semiclassical convergence of resonance states we consider as in reference [54] the Jensen–Shannon divergence [80] between quantum and classical measures,

$$d_{\text{JS}}(\mu_{\text{qm}}, \mu_{\text{cl}}) = H\left(\frac{\mu_{\text{qm}} + \mu_{\text{cl}}}{2}\right) - \frac{H(\mu_{\text{qm}}) + H(\mu_{\text{cl}})}{2}, \tag{37}$$

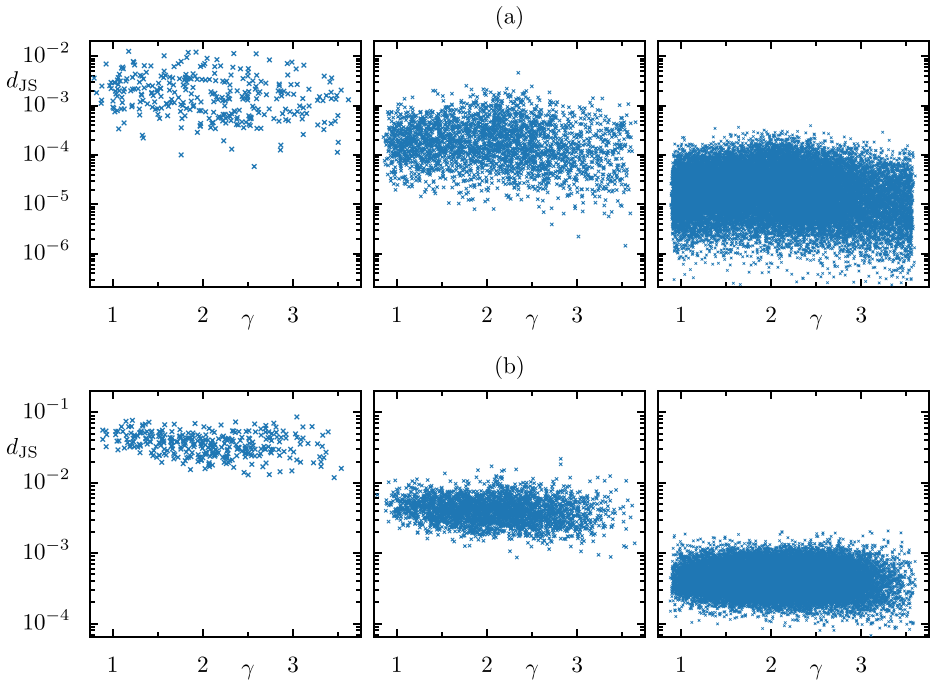

Figure 6. Jensen–Shannon divergence d_{JS} between quantum and classical measures vs γ for baker map with $\boldsymbol{r} = (0.2, 0.01, 1)$ and randomization on level (a) $(\ell_p, \ell_q) = (0, 1)$ for increasing $N \in \{315, 2835, 25\,515\}$, and (b) $(\ell_p, \ell_q) = (1, 2)$ for $N \in \{324, 2835, 25\,515\}$ evaluated on level $\ell = \ell_q$.

where H is the Shannon entropy

$$H(\mu) = -\sum_{\boldsymbol{\alpha}_{\ell,\ell}} \mu([\boldsymbol{\alpha}_{\ell,\ell}]) \ln \mu([\boldsymbol{\alpha}_{\ell,\ell}]), \tag{38}$$

evaluated on rectangles $[\boldsymbol{\alpha}_{\ell,\ell}]$ on level ℓ. The quantum measure μ_{qm} is determined by the projected weights $w_{\psi_i}([\boldsymbol{\alpha}_{\ell,\ell}])$ of a resonance state ψ_i and the classical measure μ_{cl} is given by $\mu_\gamma^{\ell_p,\ell_q}$ for $\gamma = \gamma_i$. The square root of d_{JS} is a distance on the set of measures. Weak convergence of the quantum measure to the classical measure implies that for finite ℓ the Jensen–Shannon entropy must converge to zero in the semiclassical limit $N \to \infty$.

In figure 6 we illustrate d_{JS} versus γ for increasing N for two different randomization levels. For all decay rates γ the Jensen–Shannon divergence decreases with increasing N. This supports the semiclassical weak convergence conjectured in section 4.3.

We remark that we tested the semiclassical conjecture qualitatively and quantitatively, for many different randomized baker maps, i.e., different n, different $\boldsymbol{r}$, and also different combinations of ℓ_p and ℓ_q. In all cases we found quantum–classical agreement in support of the semiclassical conjecture.

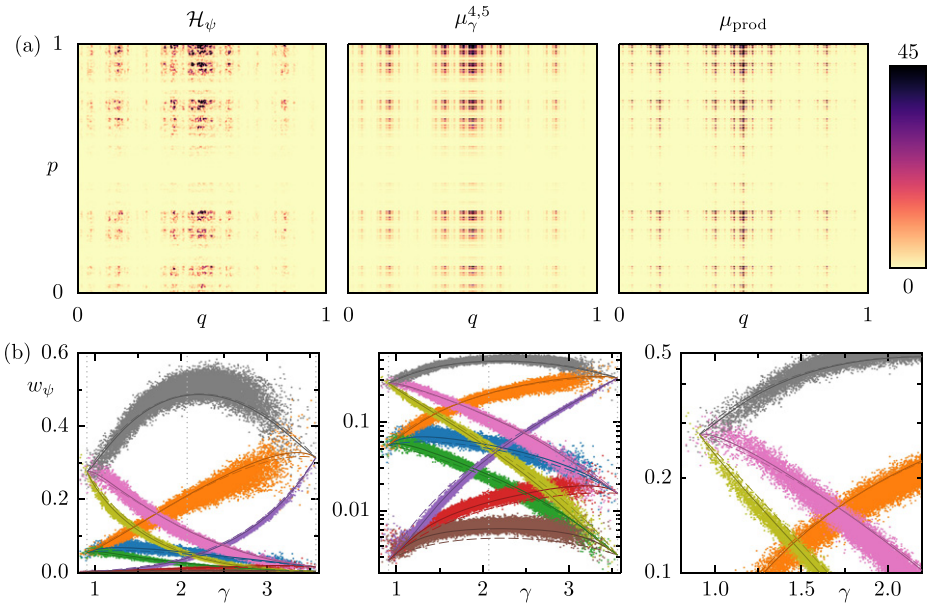

Figure 7. Deterministic three-baker map with $\boldsymbol{r} = (0.2, 0.01, 1)$ and $N = 25\,191$. (a) Husimi function of resonance state with decay rate closest to γ_{typ} (left), corresponding classical measure $\mu_\gamma^{4,5}$ (middle), and product measure μ_{prod} based on reference [54] (right). The same colormap is used for all densities. (b) Comparison of the nine projected weights $w_{\psi_i}([\boldsymbol{\alpha}_{1,1}])$ of each resonance state ψ_i (dots) to classical measures $\mu_\gamma^{4,5}$ (solid lines) and μ_{prod} (dashed lines). The same data is shown on linear (left) and logarithmic scale (middle), as well as a magnification (right).

6. Quantum baker map with escape

In this section we compare the structure of resonance states of the deterministic quantum baker map with escape, i.e., without randomization, to the randomized baker map with escape. In figure 7(a) in the left panel the Husimi function of a resonance state of the deterministic three-baker map with escape $\mathcal{B}_{n,\boldsymbol{r}}$, equation (9), is shown. This is qualitatively similar to the Husimi functions of the randomized baker map in figure 2(c) for small randomization regions. Here, we compare it to the classical measures $\mu_\gamma^{\ell_p,\ell_q}$ for even smaller randomization, $(\ell_p, \ell_q) = (4, 5)$, see middle panel in figure 7(a). These measures approximate the limit $\ell_p, \ell_q \to \infty$, see appendix B. We observe qualitative agreement between the multifractal structures of both measures.

Quantitative differences can be seen in figure 7(b), where quantum and classical weights on the rectangles $[\boldsymbol{\alpha}_{\ell,\ell}]$ with $\ell = 1$ are shown for all decay rates γ. For example, in the left panel the largest quantum weights do not scatter symmetrically around the corresponding classical weight. Similar deviations can also be seen in the right panel. Therefore the semiclassical limit measures $\mu_\gamma^{\ell_p,\ell_q}$ of the randomized baker map just approximately describe resonance states of the deterministic baker map. Numerics suggest that this does not change, neither for larger N in the baker map with escape, nor for classical measures with larger ℓ_p, ℓ_q, see appendix B.

Additionally, figure 7 shows a comparison to the product measures, proposed as approximate descriptions of resonance states in reference [54]. In figure 7(a) in the right panel the product measure visually shows differences on small scales. In figure 7(b), where the product

measure is shown as a dashed line, it deviates substantially, e.g., in the middle panel for the smallest weight at intermediate γ.

There are two main conclusions from the comparison of the baker map with and without randomization. First of all, in both systems resonance states have qualitatively similar multifractal structures on scales larger than the scale of randomization. In fact, the classical measures describing the resonance states of the randomized baker map also give the best available description for the deterministic baker map. Secondly, however, we observe that these systems have slightly different structures of their resonance states, even when the scale of randomization is chosen very small. Thus it remains open, if and how the local random vector model and the classical measures $\mu_\gamma^{\ell_p,\ell_q}$ can be generalized to deterministic chaotic systems.

7. Conclusions and outlook

In conclusion, we derive a semiclassical description for resonance states of randomized baker maps with escape based on conditional invariance and a local random vector model. We present numerical support which indicates that the conjectured measures $\mu_\gamma^{\ell_p,\ell_q}$ are indeed the semiclassical limit measures.

This model with randomization acts as a bridge towards a full understanding of resonance states in deterministic chaotic systems with escape. The following generalizations are of interest: (i) the limit from partial to full escape can be investigated for the randomized baker map and compared with the existing approximative description for systems with full escape [53]. To this end the local random vector model must be adapted to the fractal support of resonance states in systems with full escape. (ii) Generalized baker maps with stripes of arbitrary width allow for studying non-uniformly hyperbolic systems. The randomization regions could either be given by finite symbolic sequences of this map leading to different sizes (and straightforward modifications of the local random vector model) or be given by regions of identical sizes as in this work. (iii) Randomization of other chaotic maps and for smooth reflectivity functions, as they occur in optical microcavities, should be studied. Classical measures, based on the local random vector model and conditional invariance, might again perfectly describe their resonance states. Furthermore, these classical measures might give rise to the best available approximations for the resonance states of deterministic maps, similar to our observation for the baker map in section 6.

Finally, we observe that there is a quantitative difference, whether the multifractal structure of resonance states ends at the scale of a Planck cell or at the scale of randomization, even when the resonance states are compared on much larger classical scales. This insight should be helpful for future work on semiclassical theories for resonance states.

Acknowledgments

We thank A Bäcker, T Pokart, J R Schmidt, E-M Graefe, B Gutkin, M Novaes, and D V Savin for helpful comments and discussions. We would also like to thank A Bäcker, J R Schmidt, and both anonymous referees for their valuable comments and questions regarding the manuscript. This research is funded by the Deutsche Forschungsgemeinschaft (DFG, German Research Foundation)-262765445.

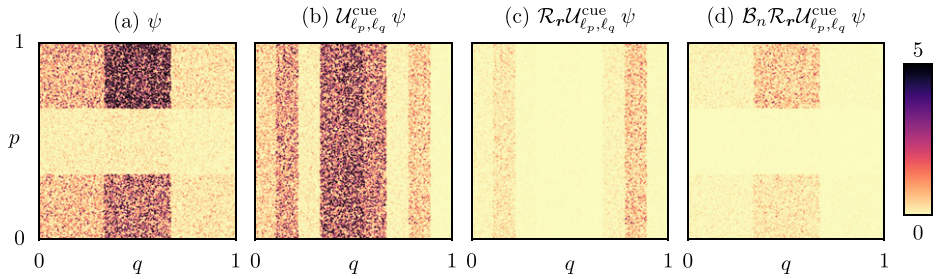

Figure A1. Husimi function of a resonance state ψ, as in figure 2(a), (left panel) and sequential application of the operators for randomization $\mathcal{U}^{\mathrm{CUE}}_{\ell_p,\ell_q}$, escape $\mathcal{R}_{\boldsymbol{r}}$, and baker map $\mathcal{B}_n$.

Data availability statement

The data that support the findings of this study are available upon reasonable request from the authors.

Appendix A. Substructure of randomization regions

In this section we discuss the observation that resonance states of the randomized baker map have substructure within the randomization regions, see figure 2 in section 3.3.

First we illustrate in figure A1 how a resonance state ψ evolves under sequential application of the operators for randomization $\mathcal{U}^{\mathrm{CUE}}_{\ell_p,\ell_q}$, escape $\mathcal{R}_{\boldsymbol{r}}$, and baker map $\mathcal{B}_n$, that appear in the randomized baker map with esape $\mathcal{B}_{n,\boldsymbol{r},\ell_p,\ell_q}$, equation (13). The same resonance state as in figure 2(a), (left panel) is used, where each of the three randomization regions is divided along the p-direction into three subregions. After application of the randomization operator, $\mathcal{U}^{\mathrm{CUE}}_{\ell_p,\ell_q}\psi$, each of the three randomization regions has again three subregions, but now along the q-direction. Application of the escape operator $\mathcal{R}_{\boldsymbol{r}}$ reduces the weight in each rectangle A_k by the factor r_k. In particular, for $\boldsymbol{r} = (0.2, 0.01, 1)$ the weight in the middle rectangle is strongly decreased. After application of the quantum baker map $\mathcal{B}_n$ the original 3×3-structure is recovered due to stretching in q-direction and compressing in p-direction. The norm, however, is reduced by a global factor e^{γ} compared to the norm of ψ.

Naively, one would expect to have no substructure in a randomization region after application of the randomization operator $\mathcal{U}^{\mathrm{CUE}}_{\ell_p,\ell_q}$. This is indeed the case, if it is applied to an arbitrary state. In figure A1, however, it is applied to an eigenstate of the randomized baker map, equation (13), making a substructure in the randomization region before and after the application of $\mathcal{U}^{\mathrm{CUE}}_{\ell_p,\ell_q}$ necessary.

Note that cyclic permutations of the three operators in $\mathcal{B}_{n,\boldsymbol{r},\ell_p,\ell_q}$ would lead to resonance states with phase-space structures corresponding to figure A1(b) or figure A1(c), while the spectrum would not change. The operators $\mathcal{U}^{\mathrm{CUE}}_{\ell_p,\ell_q}$ and $\mathcal{R}_{\boldsymbol{r}}$ commute for $\ell_q \geqslant 1$, such that their exchange neither changes spectrum nor resonance states.

Appendix B. Convergence of classical weights for $\ell_p, \ell_q \to \infty$

In the following we briefly present numerical evidence on the weak convergence of the classical measures $\mu_\gamma^{\ell_p,\ell_q}$ for increasing ℓ_p and ℓ_q. Fixing a set $A \subset \mathbb{T}$ we are interested if the limit

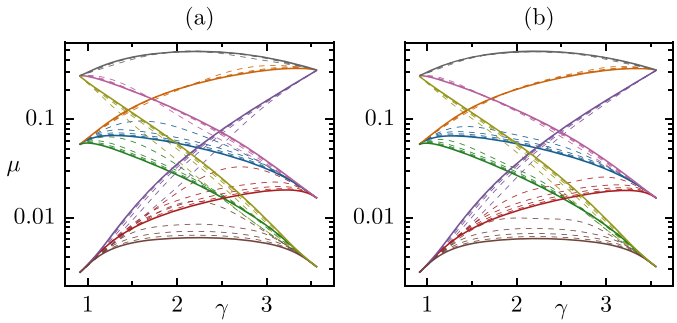

Figure B1. Convergence of classical weights $\mu_\gamma^{\ell_p,\ell_q}([\boldsymbol{\alpha}_{\ell,\ell}])$ with $\ell = 1$ for $\boldsymbol{r} = (0.2, 0.01, 1)$ and randomization on (a) $\ell_p \in \{0, 1, 2, 3, 4\}$, $\ell_q = \ell_p + 1$, and (b) $\ell_p \in \{1, 2, 3, 4, 5\}$, $\ell_q = \ell_p$. Solid lines correspond to the largest ℓ_p.

$\lim_{\ell_p,\ell_q\to\infty}\mu_\gamma^{\ell_p,\ell_q}(A)$ exists. For simplicity A is chosen as one of the rectangles $[\boldsymbol{\alpha}_{\ell,\ell}]$ at $\ell = 1$ in the following.

In figure B1 we illustrate the convergence of these classical weights versus γ for increasing level of randomization. We consider the cases (a) $\ell_q = \ell_p + 1$ and (b) $\ell_q = \ell_p$ for increasing ℓ_p. We observe that these curves converge already for the small ℓ_p presented here. Furthermore, the classical measures for the largest ℓ_p agree very well between (a) and (b). This suggests, that there is a unique limit measure, μ_γ^*, towards which $\mu_\gamma^{\ell_p,\ell_q}$ converges weakly, regardless how the limit $\ell_p, \ell_q \to \infty$ is taken. A proof of this observation is an open task.

Appendix C. Random matrix model with partial escape

In this section we apply the local random vector model combined with conditional invariance to resonance states of a random matrix model with partial escape. This leads to a straightforward derivation of the analytic expressions for their structure and its dependence on γ, given in reference [56, appendix D].

Such models are defined as the composition of a random matrix and an escape operator [56, 75, 81–83],

$$\mathcal{U}_{\boldsymbol{r}} := \mathcal{U}^{\mathrm{CUE}}_{\ell_p=0,\ell_q=0}\,\mathcal{R}_{\boldsymbol{r}}, \tag{C.1}$$

i.e., randomization takes place on the entire phase space, $\ell_p = 0$, $\ell_q = 0$. Here we consider a reflectivity operator $\mathcal{R}_{\boldsymbol{r}}$ with constant escape from the rectangles A_k, see equation (8). Resonance states are uniformly fluctuating in subregions given by the rectangles A_k, see figure C1(a), even though randomization takes place on the whole phase space.

We describe the structure of these resonance states by a classical measure μ that is constant on each rectangle A_k with weight

$$\mu_k := \mu(A_k). \tag{C.2}$$

According to the local random vector model, equation (34), we maximize the product of relative weights,

$$\Pi(\mu) = \prod_{k=0}^{n-1} \frac{\mu_k}{\sum_{l=0}^{n-1}\mu_l} = \prod_{k=0}^{n-1}\mu_k, \tag{C.3}$$

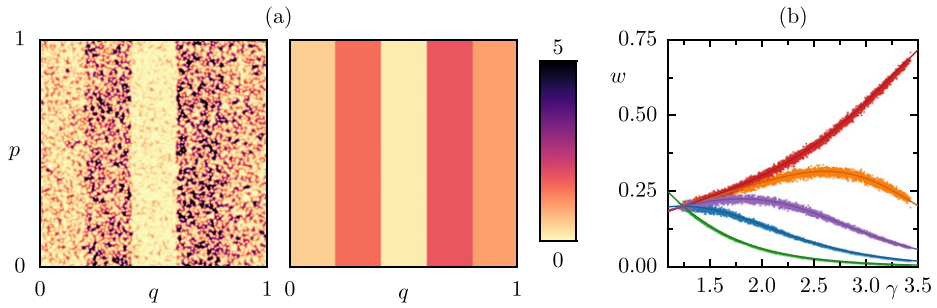

Figure C1. Random matrix with partial escape from five vertical stripes, $\boldsymbol{r} = (0.3, 0.03, 1, 0.01, 0.1)$ and $N = 5000$. (a) Husimi function of resonance state with decay rate closest to γ_{typ} (left) and classical measure μ based on local random vector model (right), using the same colormap. (b) Comparison of the five projected weights $w_{\psi_i}([\boldsymbol{\alpha}_{0,1}])$ of each resonance state ψ_i vs its decay rate γ_i (dots) to classical weights μ_k (solid lines).

where normalization $\sum_{k=0}^{n-1}\mu_k = 1$ is used (and actually a global random vector model). The constraint of conditional invariance follows from equation (18) applied to the entire phase space $\mathbb{T}$,

$$\sum_{k=0}^{n-1} r_k\,\mu_k = \mathrm{e}^{-\gamma}\sum_{k=0}^{n-1}\mu_k \qquad \Leftrightarrow \qquad \sum_{k=0}^{n-1}(\mathrm{e}^{\gamma}\,r_k - 1)\mu_k = 0. \tag{C.4}$$

Using the method of Lagrange multipliers we define a cost function maximizing $\ln\Pi(\mu)$

$$f(\{\mu_k\}) = \sum_{k=0}^{n-1}\ln\,\mu_k - \lambda\left(\sum_{k=0}^{n-1}\mu_k - 1\right) - \nu\left(\sum_{k=0}^{n-1}(\mathrm{e}^{\gamma}\,r_k - 1)\mu_k\right), \tag{C.5}$$

with Lagrange multipliers λ and ν. Setting the partial derivatives $(\partial/\partial\mu_k)f(\{\mu_k\})$ to zero we get a set of n equations,

$$\frac{1}{\mu_k} - \lambda - \nu\,(\mathrm{e}^{\gamma}\,r_k - 1) = 0. \tag{C.6}$$

Multiplying each equation by μ_k and summing over all k gives $\lambda = n$. The weights μ_k are thus given by,

$$\mu_k = \frac{1}{n + \nu(\mathrm{e}^{\gamma}\,r_k - 1)}. \tag{C.7}$$

This agrees with the expression for the density in reference [56, equation (D10)], while equation (C.4) agrees with reference [56, equation (D9)] and can be used for determining the remaining Lagrange multiplier ν corresponding to the variable ξ^* in reference [56] (up to a factor n).

In figure C1 we illustrate the structure of resonance states of a random matrix with escape from $n = 5$ rectangles. In (a) the Husimi function (left) and the corresponding classical measure μ (right) are shown for γ_{typ}. In (b) agreement of quantum and classical weights for all γ and all five rectangles A_k is demonstrated.

ORCID iDs

Konstantin Clauß https://orcid.org/0000-0003-3600-8947
Roland Ketzmerick https://orcid.org/0000-0002-2518-9343

References

[1] Haake F, Gnutzmann S and Kuś M 2018 *Quantum Signatures of Chaos* (*Springer Series in Synergetics*) (Berlin: Springer)
[2] Berry M V 1977 Regular and irregular semiclassical wavefunctions *J. Phys. A: Math. Gen.* **10** 2083–91
[3] Percival I C 1977 *Semiclassical Theory of Bound States* vol 36 (New York: Wiley) pp 1–61
[4] Voros A 1979 Semi-classical ergodicity of quantum eigenstates in the Wigner representation *Stochastic Behavior in Classical and Quantum Hamiltonian Systems* (*Lecture Notes in Physics* vol 93) ed G Casati and J Ford (Berlin: Springer) pp 326–33
[5] Shnirelman A I 1974 Ergodic properties of eigenfunctions *Usp. Math. Nauk* **29** 181–2 (in Russian)
[6] Colin de Verdière Y 1985 Ergodicité et fonctions propres du laplacien *Commun. Math. Phys.* **102** 497–502 (in French)
[7] Zelditch S 1987 Uniform distribution of eigenfunctions on compact hyperbolic surfaces *Duke. Math. J.* **55** 919–41
[8] Zelditch S and Zworski M 1996 Ergodicity of eigenfunctions for ergodic billiards *Commun. Math. Phys.* **175** 673–82
[9] Bäcker A, Schubert R and Stifter P 1998 Rate of quantum ergodicity in Euclidean billiards *Phys. Rev.* E **57** 5425–47
Bäcker A, Schubert R and Stifter P 1998 Rate of quantum ergodicity in Euclidean billiards *Phys. Rev.* E **58** 5192
[10] Esposti M D, Graffi S and Isola S 1995 Classical limit of the quantized hyperbolic toral automorphisms *Commun. Math. Phys.* **167** 471–507
[11] Bouzouina A and De Bièvre S 1996 Equipartition of the eigenfunctions of quantized ergodic maps on the torus *Commun. Math. Phys.* **178** 83–105
[12] Nonnenmacher S and Voros A 1998 Chaotic eigenfunctions in phase space *J. Stat. Phys.* **92** 431–518
[13] McDonald S W and Kaufman A N 1988 Wave chaos in the stadium: statistical properties of short-wave solutions of the Helmholtz equation *Phys. Rev.* A **37** 3067–86
[14] Aurich R and Steiner F 1991 Exact theory for the quantum eigenstates of a strongly chaotic system *Physica* D **48** 445–70
[15] Li B and Robnik M 1994 Statistical properties of high-lying chaotic eigenstates *J. Phys. A: Math. Gen.* **27** 5509–23
[16] Prosen T 1997 Quantization of generic chaotic 3D billiard with smooth boundary: II. Structure of high-lying eigenstates *Phys. Lett.* A **233** 332–42
[17] Izrailev F M 1987 Chaotic structure of eigenfunctions in systems with maximal quantum chaos *Phys. Lett.* A **125** 250–2
[18] Kus M, Mostowski J and Haake F 1988 Universality of eigenvector statistics of kicked tops of different symmetries *J. Phys. A: Math. Gen.* **21** L1073–7
[19] Bäcker A 2003 Numerical aspects of eigenvalues and eigenfunctions of chaotic quantum systems *The Mathematical Aspects of Quantum Maps* (*Lecture Notes in Physics* vol 618) ed M Degli Esposti and S Graffi (Berlin: Springer) pp 91–144
[20] Bies W E, Lepore N and Heller E J 2003 Quantum billiards and constrained random wave correlations *J. Phys. A: Math. Gen.* **36** 1605–13
[21] Urbina J D and Richter K 2003 Supporting random wave models: a quantum mechanical approach *J. Phys. A: Math. Gen.* **36** L495–502
[22] Urbina J D and Richter K 2006 Statistical description of eigenfunctions in chaotic and weakly disordered systems beyond universality *Phys. Rev. Lett.* **97** 214101
[23] Bäcker A and Schubert R 2002 Amplitude distribution of eigenfunctions in mixed systems *J. Phys. A: Math. Gen.* **35** 527–38
[24] Bäcker A and Nonnenmacher S Restricted random vector models and eigenvector statistics in systems with a mixed phase space (in preparation)

[25] Altmann E G, Portela J S E and Tél T 2013 Leaking chaotic systems *Rev. Mod. Phys.* **85** 869–918
[26] Gaspard P and Rice S A 1989 Exact quantization of the scattering from a classically chaotic repellor *J. Chem. Phys.* **90** 2255–62
[27] Wirzba A 1999 Quantum mechanics and semiclassics of hyperbolic n-disk scattering systems *Phys. Rep.* **309** 1–116
[28] Weich T, Barkhofen S, Kuhl U, Poli C and Schomerus H 2014 Formation and interaction of resonance chains in the open three-disk system *New J. Phys.* **16** 033029
[29] Cao H and Wiersig J 2015 Dielectric microcavities: model systems for wave chaos and non-Hermitian physics *Rev. Mod. Phys.* **87** 61–111
[30] Sjöstrand J 1990 Geometric bounds on the density of resonances for semiclassical problems *Duke Math. J.* **60** 1–57
[31] Lin K K 2002 Numerical study of quantum resonances in chaotic scattering *J. Comput. Phys.* **176** 295–329
[32] Lu W T, Sridhar S and Zworski M 2003 Fractal Weyl laws for chaotic open systems *Phys. Rev. Lett.* **91** 154101
[33] Schomerus H and Tworzydło J 2004 Quantum-to-classical crossover of quasibound states in open quantum systems *Phys. Rev. Lett.* **93** 154102
[34] Ramilowski J A, Prado S D, Borondo F and Farrelly D 2009 Fractal Weyl law behavior in an open Hamiltonian system *Phys. Rev.* E **80** 055201(R)
[35] Eberspächer A, Main J and Wunner G 2010 Fractal Weyl law for three-dimensional chaotic hard-sphere scattering systems *Phys. Rev.* E **82** 046201
[36] Ermann L and Shepelyansky D L 2010 Ulam method and fractal Weyl law for Perron–Frobenius operators *Eur. Phys. J.* B **75** 299–304
[37] Pedrosa J M, Wisniacki D, Carlo G G and Novaes M 2012 Short periodic orbit approach to resonances and the fractal Weyl law *Phys. Rev.* E **85** 036203
[38] Nonnenmacher S, Sjöstrand J and Zworski M 2014 Fractal Weyl law for open quantum chaotic maps *Ann. Math.* **179** 179–251
[39] Wiersig J and Main J 2008 Fractal Weyl law for chaotic microcavities: Fresnel's laws imply multifractal scattering *Phys. Rev.* E **77** 036205
[40] Nonnenmacher S and Schenck E 2008 Resonance distribution in open quantum chaotic systems *Phys. Rev.* E **78** 045202(R)
[41] Gutkin B and Osipov V A 2015 Universality in spectral statistics of open quantum graphs *Phys. Rev.* E **91** 060901(R)
[42] Schönwetter M and Altmann E G 2015 Quantum signatures of classical multifractal measures *Phys. Rev.* E **91** 012919
[43] Casati G, Maspero G and Shepelyansky D L 1999 Quantum fractal eigenstates *Physica* D **131** 311–6
[44] Lee S-Y, Rim S, Ryu J-W, Kwon T-Y, Choi M and Kim C-M 2004 Quasiscarred resonances in a spiral-shaped microcavity *Phys. Rev. Lett.* **93** 164102
[45] Keating J P, Novaes M, Prado S D and Sieber M 2006 Semiclassical structure of chaotic resonance eigenfunctions *Phys. Rev. Lett.* **97** 150406
[46] Nonnenmacher S and Rubin M 2007 Resonant eigenstates for a quantized chaotic system *Nonlinearity* **20** 1387–420
[47] Keating J P, Nonnenmacher S, Novaes M and Sieber M 2008 On the resonance eigenstates of an open quantum baker map *Nonlinearity* **21** 2591–624
[48] Novaes M, Pedrosa J M, Wisniacki D, Carlo G G and Keating J P 2009 Quantum chaotic resonances from short periodic orbits *Phys. Rev.* E **80** 035202(R)
[49] Harayama T and Shinohara S 2015 Ray-wave correspondence in chaotic dielectric billiards *Phys. Rev.* E **92** 042916
[50] Körber M J, Bäcker A and Ketzmerick R 2015 Localization of chaotic resonance states due to a partial transport barrier *Phys. Rev. Lett.* **115** 254101
[51] Carlo G G, Benito R M and Borondo F 2016 Theory of short periodic orbits for partially open quantum maps *Phys. Rev.* E **94** 012222
[52] Kullig J and Wiersig J 2016 Frobenius–Perron eigenstates in deformed microdisk cavities: non-Hermitian physics and asymmetric backscattering in ray dynamics *New J. Phys.* **18** 015005
[53] Clauß K, Körber M J, Bäcker A and Ketzmerick R 2018 Resonance eigenfunction hypothesis for chaotic systems *Phys. Rev. Lett.* **121** 074101
[54] Clauß K, Altmann E G, Bäcker A and Ketzmerick R 2019 Structure of resonance eigenfunctions for chaotic systems with partial escape *Phys. Rev.* E **100** 052205

[55] Bittner S, Kim K, Zeng Y, Wang Q J and Cao H 2020 Spatial structure of lasing modes in wave-chaotic semiconductor microcavities *New J. Phys.* **22** 083002
[56] Clauß K, Kunzmann F, Bäcker A and Ketzmerick R 2021 Universal intensity statistics of multifractal resonance states *Phys. Rev.* E **103** 042204
[57] Demers M F and Young L-S 2006 Escape rates and conditionally invariant measures *Nonlinearity* **19** 377–97
[58] Kopp M and Schomerus H 2010 Fractal Weyl laws for quantum decay in dynamical systems with a mixed phase space *Phys. Rev.* E **81** 026208
[59] Körber M J, Michler M, Bäcker A and Ketzmerick R 2013 Hierarchical fractal Weyl laws for chaotic resonance states in open mixed systems *Phys. Rev. Lett.* **111** 114102
[60] Malzard S, Poli C and Schomerus H 2015 Topologically protected defect states in open photonic systems with non-Hermitian charge-conjugation and parity-time symmetry *Phys. Rev. Lett.* **115** 200402
[61] Mudute-Ndumbe S and Graefe E-M 2020 A non-Hermitian PT-symmetric kicked top *New J. Phys.* **22** 103011
[62] Weber J, Haake F and Šeba P 2000 Frobenius–Perron resonances for maps with a mixed phase space *Phys. Rev. Lett.* **85** 3620–3
[63] Weber J, Haake F, Braun P A, Manderfeld C and Šeba P 2001 Resonances of the Frobenius–Perron operator for a Hamiltonian map with a mixed phase space *J. Phys. A: Math. Gen.* **34** 7195–211
[64] Manderfeld C, Weber J and Haake F 2001 Classical versus quantum time evolution of (quasi-)probability densities at limited phase-space resolution *J. Phys. A: Math. Gen.* **34** 9893–905
[65] Albeverio S, Haake F, Kurasov P, Kuś M and Šeba P 1996 S-matrix, resonances, and wave functions for transport through billiards with leads *J. Math. Phys.* **37** 4888–903
[66] Hackenbroich G, Viviescas C and Haake F 2003 Quantum statistics of overlapping modes in open resonators *Phys. Rev.* A **68** 063805
[67] Haake F 1973 *Statistical Treatment of Open Systems by Generalized Master Equations* (*Springer Tracts in Modern Physics* vol 66) ed G Höhler (Berlin: Springer) pp 98–168
[68] Strunz W T and Haake F 2003 Decoherence scenarios from microscopic to macroscopic superpositions *Phys. Rev.* A **67** 022102
[69] Lai Y-C and Tél T 2011 *Transient Chaos: Complex Dynamics on Finite Time Scales* (*Applied Mathematical Sciences* vol 173) 1st edn (New York: Springer)
[70] Arnold V I and Avez A 1968 *Ergodic Problems of Classical Mechanics* (New York: Benjamin)
[71] Altmann E G, Portela J S E and Tél T 2015 Chaotic explosions *Europhys. Lett.* **109** 30003
[72] Altmann E G, Portela J S E and Tél T 2013 Chaotic systems with absorption *Phys. Rev. Lett.* **111** 144101
[73] Balazs N L and Voros A 1989 The quantized Baker's transformation *Ann. Phys., NY* **190** 1–31
[74] Saraceno M 1990 Classical structures in the quantized baker transformation *Ann. Phys., NY* **199** 37–60
[75] Fyodorov Y V and Sommers H-J 1997 Statistics of resonance poles, phase shifts and time delays in quantum chaotic scattering: random matrix approach for systems with broken time-reversal invariance *J. Math. Phys.* **38** 1918–81
[76] Schomerus H 2013 From scattering theory to complex wave dynamics in non-Hermitian $\mathcal{PT}$-symmetric resonators *Phil. Trans. R. Soc.* A **371** 20120194
[77] Husimi K 1940 Some formal properties of the density matrix *Proc. Phys. Math. Soc. Japan* **22** 264–314
[78] Brody T A, Flores J, French J B, Mello P A, Pandey A and Wong S S M 1981 Random-matrix physics: spectrum and strength fluctuations *Rev. Mod. Phys.* **53** 385–479
[79] Marklof J, O'Keefe S and Zelditch S 2005 Weyl's law and quantum ergodicity for maps with divided phase space (with an appendix converse quantum ergodicity) *Nonlinearity* **18** 277–304
[80] Grosse I, Bernaola-Galván P, Carpena P, Román-Roldán R, Oliver J and Stanley H E 2002 Analysis of symbolic sequences using the Jensen–Shannon divergence *Phys. Rev.* E **65** 041905
[81] Fyodorov Y V and Sommers H-J 2000 Spectra of random contractions and scattering theory for discrete-time systems *J. Exp. Theor. Phys. Lett.* **72** 422–6
[82] Zyczkowski K and Sommers H-J 2000 Truncations of random unitary matrices *J. Phys. A: Math. Gen.* **33** 2045–57
[83] Bogomolny E 2010 Asymptotic mean density of sub-unitary ensembles *J. Phys. A: Math. Theor.* **43** 335102